Shahrood University of Technology
Iranian Society of Mining Engineering (IRSME)
Journal of Mining and Environment (JME)
journal homepage: www.jme.shahroodut.ac.ir
THOMSON REUTERS
Vol. 10, No. 3, 2019, 747-762.
DOI: 10.22044/jme.2019.8203.1695

Anomaly delineation of porphyry copper deposits of Hanza region through geochemical data analysis and multi-spectral remote sensing

A. Habibnia, G.R. Rahimipour* and H. Ranjbar

Department of Mining Engineering, Faculty of Engineering, Shahid Bahonar University of Kerman, Kerman, Iran

Received 16 March 2019; received in revised form 28 April 2019; accepted 13 May 2019

Keywords

Hanza Region

Urumieh-Dokhtar Metallogenic Belt

Median Absolute Deviation Method

Geochemical Mapping

Porphyry Copper Deposits

ASTER

False-Colour Composite

Abstract

The Hanza region is located in the southern part of Urumieh–Dokhtar metallogenic belt in SE Iran. This region includes six known porphyry copper deposits, and it is considered as an ore-bearing region from the geochemical viewpoint. The aim of this research work is to examine the effective processing techniques in the analysis of stream sediment geochemical datasets and ASTER satellite images. The processing methods have led to the identification of eight new prospective areas. These methods are aimed at providing univariate geochemical maps. The stream sediment geochemical mapping for Cu and Mo is performed by the sample catchment basin approach. The results derived from this approach have been mapped in four classes associated with the first quartile, third quartile, and threshold values obtained from the Median Absolute Deviation method. False-colour composite and band ratio techniques are adopted as two well-known methods for the processing of an ASTER scene spanning the studied area. Eight new targets for possible mineralization have been resulted from geochemical data analysis. Image processing techniques on the ASTER multi-spectral data have also revealed widespread hydrothermal alterations associated with the known porphyry copper deposits and the new prospects.

1. Introduction

Geochemical studies are an important part of the geoscience research works to explore metallic and non-metallic mineralizations [1]. In regional mineral explorations, the stream sediment geochemical data can be effective in identifying new prospective areas and mapping geochemical patterns in regional metallogeny. They have been employed by many researchers in preliminary stages of mineral explorations [2-11]. Geochemical anomaly delineation from stream sediment dataset is a challenging task [12, 13].

Identification of mineral deposits associated with geochemical anomalies in the exploration of new mineralization is necessary, and geochemical anomalies can be direct indicators for the discovery of unknown mineralization [12, 14-17]. In geochemical data utilization, recognizing anomalous areas is a basic task [12]. The anomaly delineation in geochemical exploration surveys is based on a threshold, and the values higher than the threshold are considered as the anomaly [18]. In geochemical datasets, various methods have been introduced to set threshold for separating anomalies from background including mean+2 × standard deviation [19], Exploratory Data Analysis (EDA) [20], fractal analysis [21], and Median Absolute Deviation (MAD) [14]. In surface geochemical exploration, one should not only pay attention to the obvious anomalies (extreme outlier values), since weak anomalies may exist on the surface that could be associated with ore mineralization, whereas strong anomalies may also exist that are not related to the mineralization in depth. The following reasons could be addressed:

* Corresponding author: rahimipour@uk.ac.ir (G.R. Rahimipour).

1) Strong anomalies may be related to other lithological units (e.g. shale), 2) the alluvial cover may prevent exposing hidden deposits, 3) element concentrations may vary significantly in different deposits, 4) anthropogenic contaminations may lead to a change in the nature of geochemical features [17].

Remote sensing technology plays a significant role in the preliminary stages of mineral exploration, especially in arid and semi-arid regions. Alteration mapping through remote sensing has been broadly and successfully used for the exploration of hydrothermal deposits, particularly porphyry copper mineralization [22-29]. Remote sensing processing methods allow us to quantify alteration mineralogy and to recognize key alteration minerals and implicit chemical variations [24, 30-32]. As an important criterion, results of satellite image processing techniques can play a key role in consolidating geochemical anomalous areas.

The Regional Reconnaissance Surveys (RRSs) is the first stage of mineral exploration, and its main purpose is to reduce the areas by identifying prospects for further studies. The RRS stage is very important in identifying new mineralizations. Thus information provided at this stage could be regional geophysics (e.g. airborne geophysical surveys), geological map, remote sensing, and regional geochemical data. Exact processing at this stage can lead to the identification of new prospective areas and new mineral deposits; however, it may lead to their elimination.

As the literature admits, a few remote sensing studies using ASTER data were carried out in the southern part of the Urumieh–Dokhtar Metallogenic Belt (UDMB) [e.g. 33-38], examples of which include the following: (1) Mohebi *et al*. [33] showed the distribution of phyllic and argillic alteration zones and faults on the ASTER image (RGB; 468) in the Hanza Mountain district; (2) Mars and Rowan [34] performed logical operator algorithms based on ASTER defined band ratios for regional mapping of hydrothermal alteration zones (phyllic and argillic altered rocks) in the Zargros magmatic zone (e.g. southern part of the Central Iranian Volcanic Belt), and also they discriminated hydrothermal alterations using Relative Absorption Band Depth; (3) Tangestani *et al*. [35] evaluated ASTER satellite images for alteration zone enhancement related to porphyry copper mineralization in the southern UDMB; (4) Khaleghi and Ranjbar [36] mapped hydrothermal alteration zones associated with the porphyry copper mineralization in the Hanza Mountain district (e.g. Sarduiyeh area) using ASTER SWIR data; (5) Beiranvand Pour *et al*. [37] distinguished the sericitic, argillic, and propylitic alteration zones associated with Miduk and Sarcheshmeh PCDs in the southern UDMB using ASTER band ratio; and (6) Alimohammadi *et al*. [38] discriminated hydrothermal alteration zones related to the PCDs in the Hanza Mountain district (Daraloo–Sarmeshk area) using false colour composition of ASTER band ratio.

This paper is organized as five sections. The literature review and the aim of this research work are presented in the introduction section. The general characteristics of the area and geological features are described in the second section. The methodology section comprises several methods used for both the geochemical and remote sensing approaches. The results obtained for both remote sensing and geochemical data analysis are discussed in the results and discussion section. Finally, the conclusions are listed in the conclusion section.

2. Studied area

The Hanza region is located in the northern part of Sarduiye geological sheet with a scale of 1:100000 in the Kerman province, Iran. This area is located between longitudes 57° 00′ to 57° 30′and latitudes 29° 15′ to 29° 30′, and is a part of Urumieh –Dokhtar Magmatic Belt (UDMB), which contains many Porphyry Copper Deposits (PCDs) such as Sarcheshmeh, Miduk, Darrehzar, Sungun, and other types of mineralizations such as gold and iron [33, 39-44]. The UDMB results from the subduction of Neo-Tethys oceanic crust underneath the Iranian microcontinent and the subsequent collision of Iranian and Arabian plates in Tertiary [41, 45, 46]. The Hanza region is located in the southern part of UDMB, and this region contains the known economic PCDs including Daralu, Bondar Hanza, Sarmesk, Hanza, and Gouro (Figure 1). Mohebi *et al*. [33] studied distribution of major faults within the area. They demonstrated that the NW-SE (N125°–145°) trend was an important direction in the spatial distribution of ore deposits and in localizing the hydrothermal fluids, forming alteration zones, and constituting PCDs. This trend, which also coincides with that of the UMDB, should be considered as an important direction for the exploration of the PCDs in Kerman Cu belt. The PCDs have occurred mainly within an assemblage of normal and thrust faults in the region. The NW–SE trending faults (brownish lines in Figure

1) coincide with the PCD trend, the main thrusts in the region as well as the trend of UDMB and the trend of precursor granitoid pluton [33].

2.1. Alignments of known PCDs

According to [47], "At the regional scale, porphyry Cu systems and their contained deposits tend to occur as clusters or alignments that may attain 5 to 30 km across or in length, respectively. Clusters are broadly equi-dimensional groupings of deposits, whereas alignments are linear deposit arrays oriented either parallel or transverse to the magmatic arcs and their coincident porphyry Cu belts" (p.6). Sillitoe [47] stated that "the plutons may act as hosts to a single deposit, as at Mount Polley, British Columbia; or clusters of two or more discrete deposits, as in the El Abra intrusive complex, northern Chile; or an alignment of coalesced deposits, as in the Los Bronces-Río Blanco district" (p. 6). The Hanza region is an example of coalesced deposits that are aligned in the northwest-southeast direction. In this area, there are six known PCDs including 1-Daralu, 2-Sarmeshk, 3-Bondar Hanza, 4-Hanza, 5-Gouro, and 6-Sorakhmar from NW to SE, respectively (Figure 1). Based on the density of known PCDs scattering along a certain direction, there is a high probability of more PCD prospects in the studied area along this direction. Thus this region was selected in order to be reassessed during a national project aimed at identifying new mineral deposits, especially the Cu-Mo porphyry mineralization type.

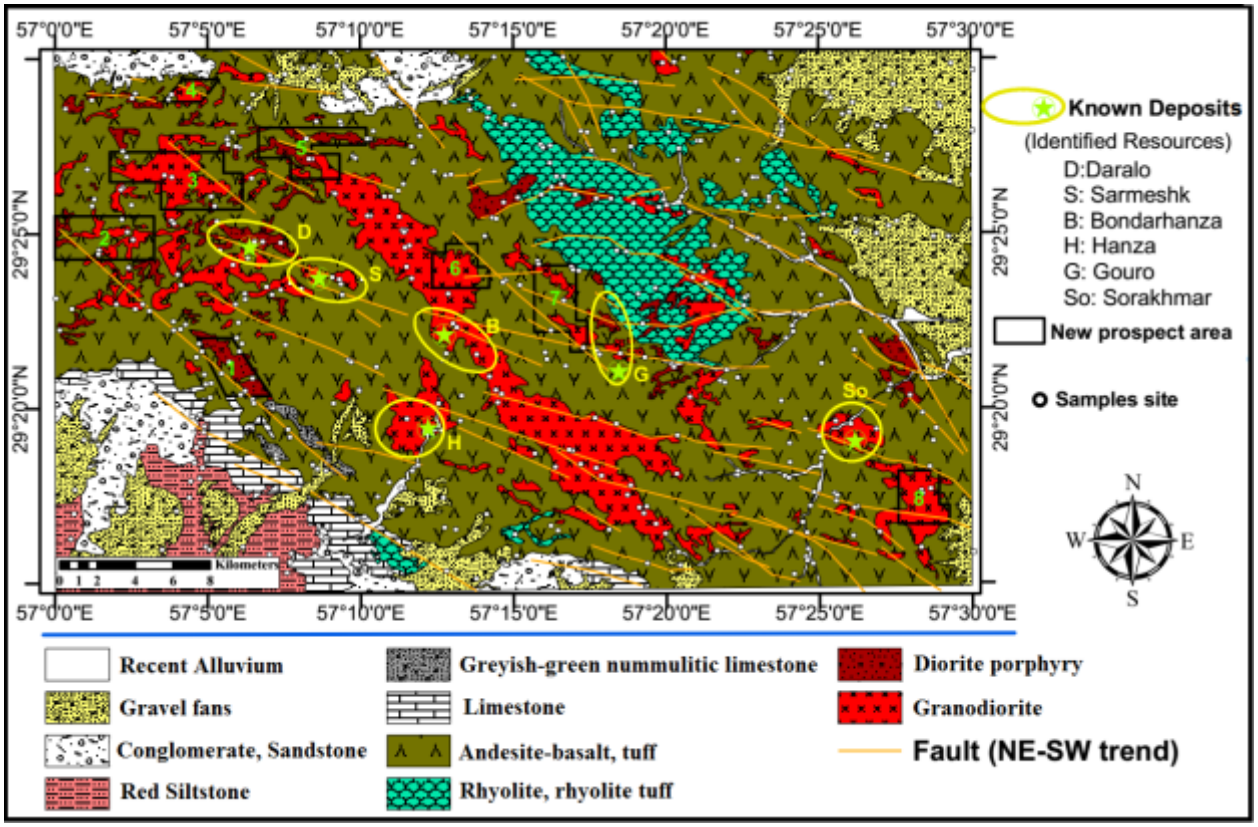

Figure 1. Geology of the Hanza region showing the locations of PCDs and faults based on 1:100,000 Serduiyeh map from the Geological Survey of Iran (modified after Djokovic et al., 1973 [42]).

2.2. Geological units

The Hanza Mountain area represents a monoclinal structure, mainly composed of middle to late Eocene volcanics. The outcrop of Eocene volcanics show a well-developed recurrence of phases, each beginning with andesite-basalt, basalt, and a small number of alkali rocks (trachyandesite, albite-trachyte) and ending with acidic types (mostly rhyolites and rhyodacites). Andesite-basalts are the most widespread. They are grey, purplish, and reddish-brown. These rocks consist of abundant plagioclase phenocrysts, augite, and totally altered olivine. The basalts have less plagioclase and contain, in addition, monoclinic pyroxene and olivine. The trachyandesites have very large phenocrysts, and some show a transition to trachyandesites-basalts. The rhyolites and rhyodacites are greyish-white in colour. The rhyolites are compact, almost aphanitic; phenocrysts show only K-feldespar and

albite, and mafic minerals are represented only by scarce contours of a mineral filled with limonite, sericite, and chlorite. Rhyodacites and dacites form rare lava flow, being represented mostly by pyroclastic. They differ from rhyolite in having quartz phenocrysts and larger quantity of mafic constituents (mostly hornblend, with very rare biotite and pyroxene) [42]. The Neogene sediments are widely extended in the south of Hanza mountains (the southernmost part of the studied area). The lowermost outcropping unit consists of reddish siltstones and fine-grained sandstones, in alternation with greyish sandstones and microconglomerates, which show a coarse lamination. The middle part is a monotonous sequence of semi-lithified greenish sandstones consisting of angular fragments of volcanic rocks. The uppermost horizon is similar to the middle one but has a reddish colour and generally coarser grain [42]. All volcanic rocks are intruded by Oligocene–Miocene granitoids. The granitoids that are mostly granodiorites, less commonly diorites, with transitions into granodiorite porphyries, diorite porphyries, and quartz diorite porphyries, are intruded by numerous mafic dykes. The major copper mineralization is associated with the intrusive rocks with granodiorite composition [33, 39, 42, 48, 49].

3. Materials and methods

Stream sediment geochemical mapping is a useful method for prospecting one a regional scale [2- 6, 13]. Four hundred fifty-one samples from north of Sardouiyeh sheet located in the Hanza region (the studied area) were selected to be assessed for identifying anomalous areas. The selection of two elements (i.e. Cu and Mo), is closely related to the porphyry type mineralization. The sample media were stream sediments, collected by Geological Survey of Iran by a sampling-density of one sample per 1.5 km^2 for Sardouiyeh sheet (Figure 1). Weights of samples analyzed ranging from 2.5 kg to 3.5 Kg and the samples were collected out of -80 mesh size (180 μ) of stream sediment. The samples were dried for 48 h in laboratory temperature and then were pulverized to 75 μ. At every stage and between every sample, hot water and compressed air were used to clean the equipment for minimizing contamination. Approximately 0.5 g of each milled sample was digested in a Teflon vessel mounted on a hot box using a four-Acid Digestion (5 mL HCl, 4 mL HNO_3, 4 mL HF, and 2 mL $HClO_4$). Each solution sample was chemically analyzed by the 735-Es Series Inductively Coupled Plasma Optical Emission Spectrometers (ICP-OES), manufactured by the Varian Company in Australia.

3.1. Sample catchment basin approach

Stream sediments associated with a catchment basin containing exposed mineralization would have higher concentrations of elements, as compared to stream sediments associated with non-mineralized basins [8]. One of the widely accepted and implemented techniques in the analysis of stream sediment geochemical datasets is the Sample Catchment Basin Approach (SCBA) [8, 50-52]. This method tries to estimate the background concentration of elements for every sample in the catchment scale. In SCBA, the geometry and boundary of every sample catchment basin are delimited by the next sample upstream; hence, the catchment basin area is known as the partial (or incremental) area (Figure 2) [8, 50, 53, 54]. In other words, the catchment basin area of every sample in this approach is not extended to its natural boundaries upstream, except for the uppermost sample for which there is no sample above (SCB 9 in Figure 2). In fact, the size of the area for a catchment basin refers to the partial size limited between two samples, as shown in figure 2 [8]. In SCBA, the geometry and boundary of every catchment basin is independent from the upstream or downstream catchment basins. For example, in Figure 2, catchment basin for the sample with code S8 is incremental catchment area between a sample site (S8) and the next sample site upstream (S9). As a result of this approach, the studied area is divided into an independent catchment basin from each sample site, and the catchment basin of the downstream sample does not merge with its upstream, and the spatial recognition of the mineralization site is more precise. In order to draw sample catchment basins, digital elevation model (DEM) of the studied area was utilized along with the stream sediment sample locations. In the construction of catchment basins, the spatial position of stream sediment samples and the drainage density map were employed, resulting in the production of a map with basins independent from each other.

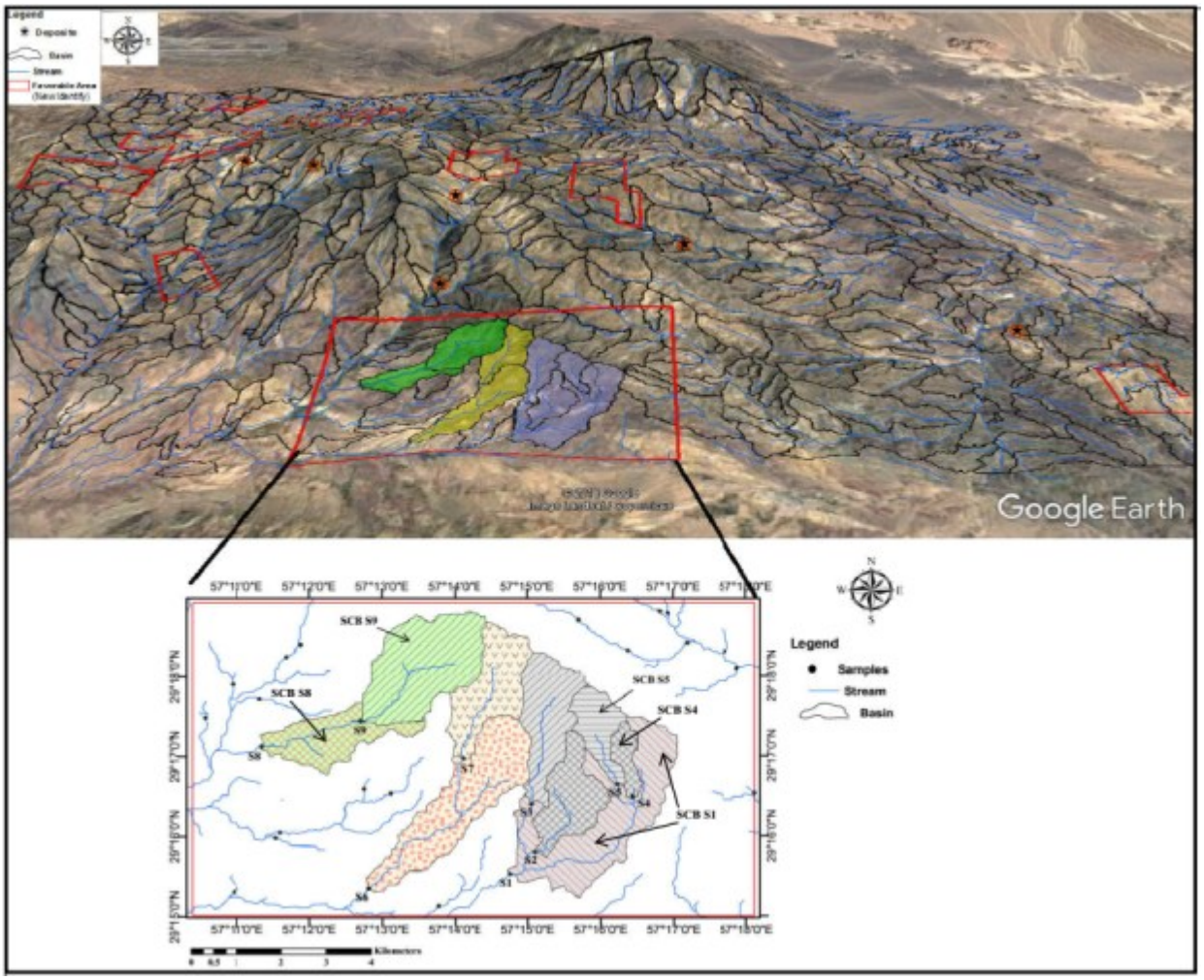

Figure 2. Partial catchment basins for the studied area in 3D view.

3.2. Threshold estimation method

Identifying geochemical anomalies in the mineral resource exploration is necessary, and geochemical anomalies can be direct indicators for the discovery of unknown mineralization [12, 14, 16, 17, 53]. In geochemical mapping, the values more than threshold are introduced as anomaly [18]. The threshold is estimated by the MAD method. To show the efficiency of this method for the identification of known PCDs and new prospective areas, the copper and molybdenum stream sediment geochemical maps were made based on SCBA.

3.2.1. Median absolute deviation method

In threshold estimation, using median and median absolute deviation (MAD) instead of mean and the standard deviation may be preferable when working with complex geochemical data (55, 56). In this method, the threshold can be defined as Median+2MAD (Eqs. 1 and 2). MAD is the median absolute deviation, which is estimated as the median of absolute deviations of all data values from the data median [14, 16, 20, 53, 55-57].

$$MAD = \text{Median}\left[\left|X_i - \text{median}(x_i)\right|\right] \quad (1)$$

$$\text{Threshold} = \text{Median} + 2MAD \quad (2)$$

where x_i is the concentration value for each sample. In threshold estimation, methods that do not strongly build on statistical assumptions should be the first choice [14]. *MAD* is analogous to *SDEV* (standard deviation) in classical statistics, so median+2*MAD* threshold is analogous to the classical mean+2*SDEV* threshold. In the MAD method, the threshold is precisely and quickly estimated by fixed formulas, and through determining parameters such as Q2 and MAD, the result of estimation does not depend on an expert's judgment.

3.3. Remote sensing

PCDs are typically characterized by zoned assemblages of hydrothermal alteration minerals (Figure 3) [34, 58]. These minerals represent

spectral reflection and absorption features in the different wavelength regions [34, 59, 60]. Multi-spectral images with sufficient spectral and spatial resolution to determine spectral absorption/reflection features can be used to identify and remotely map hydrothermal alteration zones [34]. Argillic and phyllic hydrothermal alterations associated with porphyry systems are surrounding the porphyry systems (Figure 3) [34, 47]. Alteration zones are formed in a wide range of geological environments such as volcano-plutonic rocks and with hydrothermal mineral deposits, which can be the exploratory targets [61]. Argillic alteration is characterized by the formation of clay minerals due to intense H^+ metasomatism and acid leaching [62]. Kaolinite, pyrophylite, montmorlionite, and alunite are the common hydrothermal alteration minerals in this zone. Phyllic or quartz-sericite alteration is typified by the assemblage quartz-sericite-pyrite (QSP). The phyllic alteration is one of the most common types of hydrothermal alteration as it is present in almost all hydrothermal mineral deposits, especially PCDs [62]. Muscovite is the indicator mineral in this zone that can be detected by remote sensing techniques.

Key minerals of argillic and phyllic alterations were identified by remote sensing techniques based on their spectral characteristics. ASTER is a multi-spectral imaging sensor that measures the reflected and emitted electromagnetic radiation from the Earth's surface and atmosphere in 14 bands [37]. The ASTER data used in this work was obtained from https://earthexplorer.usgs.gov/ and consisted of level 1T ASTER scenes of the studied area in the southeastern part of the Central Iranian Volcanic Belt. The images were acquired on July 13, 2005. The images were georeferenced to UTM zone 40 North projection using WGS-84 as datum. The Internal Average Relative Reflection (IARR) correction was performed on these images as atmospheric correction based on the procedure by [63]. False-Colour Composite and Band Ratio techniques were adopted as two well-known methods for the processing of ASTER images of the studied area.

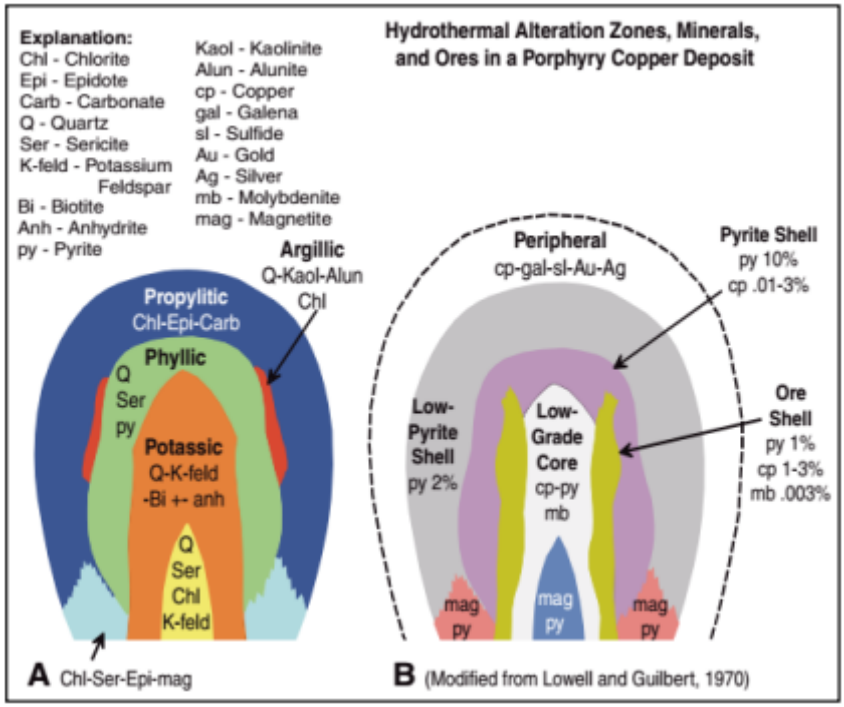

Figure 3. Illustrated deposit model of a porphyry copper deposit [34]. (A) Schematic cross-section of hydrothermal alteration minerals and types, which include propylitic, phyllic, argillic, and potassic alteration. (B) Schematic cross-section of ores associated with each alteration type.

3.3.1. False- colour composite (FCC) method

Most of the satellite imageries are in the form of multi-bands. Analyzing a band cannot alone provide the maximum of information, and the use of colour composite images of multi-bands is common and can provide ample geological information [64, 65]. For any band of multi-spectral image, the interpreter can assign a display colour, and it is done in freewill ways. In the displayed image, the colour of an object does not have any similarity with its true colour and is known as a false colour composite (FCC) image

[66]. The displayed colour for each image also may not match the actual wavelength for that colour. Many band combinations are possible but convention logic and information requirements will dictate those that are most useful [67]. By using colour composite image in Red-Green-Blue (RGB) with band combinations, it is possible to construct images that differentiate some surface materials (e.g. different lithological units) based on colour variation [67]. FCC images have been created and used by many researchers for hydrothermal alteration mapping [68, 69]. The interpretation of FCC images depends on how these bands are assigned to the three principal colours in Red, Green and Blue [70].

3.3.2. Band ratio (BR) method

The BR transformation of ASTER data is a powerful technique for visualizing the anomalies and quantitative detection of hydrothermal alteration minerals [24, 59, 68]. It is a technique where the digital number (DN) value of one band is divided by the corresponding DN value of another band. BRs are a useful technique for detection of some features that cannot be seen in the raw bands [29, 71]. The ASTER BR technique has also reported wide acceptance in mineral exploration in the recent years, and ratio images display the spectral contrast of absorption and reflection features in order to identify hydrothermal alteration minerals [29, 30, 34, 72-74]. Selected ASTER VNIR and SWIR bands have been used for BR in this work. The ASTER BR and Relative absorption Band Depth image (RBD; [75]) methods are useful in hydrothermal alteration mapping and also lithological mapping [68]. The ASTER RBD images are useful for displaying Al-O-H, Fe, Mg-O-H, and CO_3 absorption intensities. For each absorption feature, the numerator is the sum of two reflection bands, and the denominator band is the nearest position to the minimum absorption feature [34, 75].

4. Results and discussion

4.1. Geochemical dataset processing

There are 14 significant anomalous areas that include six known PCDs and eight new prospective areas of copper-molybdenum porphyry mineralization. Copper and molybdenum elements, as indicator elements, are extensively used in exploring copper-molybdenum porphyry systems by many researchers [47, 76-78]. It is vital to have geochemical maps of these elements and also determine their anomalous areas to identify promising areas. Thus to identify anomalous areas, the copper and molybdenum stream sediment geochemical maps have been made based on SCBA in four classes associated with the first quartile, third quartile, and threshold values obtained from Median Absolute Deviation method (Figure 4). Class 1: values less than the first quartile as low background, Class 2: values between the first quartile and the third quartile as background, Class 3: between the third quartile and the threshold value as high background, Class 4: values more than the threshold as anomaly. The threshold of Cu and Mo elements was estimated by the MAD method. This method is independent from the element distribution. In this method, all data values must be included in calculation for accurate calculation of the absolute deviation. The results of this method are shown in Table 1. In this research work, the efficiency of the MAD method is determined based on the "***success rate***", which is defined as below:

$$Success\ Rate = \left(\frac{NS}{NT}\right) \times 100$$

N_S = Sum of identified anomalous areas, N_T = Total of known anomalous areas

Success Rate	Efficiency
80-100%	Very high
60-80%	High
50-60%	Fairly high
40-50%	Fairly low
20-40%	Low
<20%	Very low

The success rate in the following table shows the efficiency of the MAD method in identifying anomalous areas (Table 2). It is worth noting that the *success rate* in identifying an anomalous area depends on different factors as below but these factors are considered the same and fixed in this paper. These factors are 1- Appropriate design of sampling grid 2- Spatial position of sampling points relative to anomalous areas.

The principle of the MAD technique is unlike the conventional statistical techniques because it does not require a dataset to follow normal distribution.

In this work, the success rate of the MAD method in identifying anomalous areas is 86 % and 93% for Cu and Mo, respectively (Table 2). Six known PCDs (i.e. Daralu, Sarmeshk, etc.) have been identified as anomalous areas in the stream sediment geochemical map of molybdenum. The efficiency of the MAD method in the threshold estimation and recognizing the mineralization areas, as anomaly, is high. Amongst six known PCDs, with economic value, copper anomalies were not visible in the Hanza and Sorakhmar deposits but molybdenum anomalies became apparent in all deposits. Whilst among the eight new prospective areas (i.e. polygons no. 1-8), molybdenum anomaly was not visible only in polygon 1, and in the remained polygons, both copper and molybdenum anomalies became apparent, which could indicate the very high efficiency of the MAD method for identifying new mineralization areas.

Table 1. Results of threshold estimation by MAD method.

	Cu	Mo
Median (Q2)	34.5	0.81
$\boldsymbol{MAD = Median\,[\,\lvert Xi - Q2\rvert\,]}$	5.08	0.10
Threshold	44.73	1.02

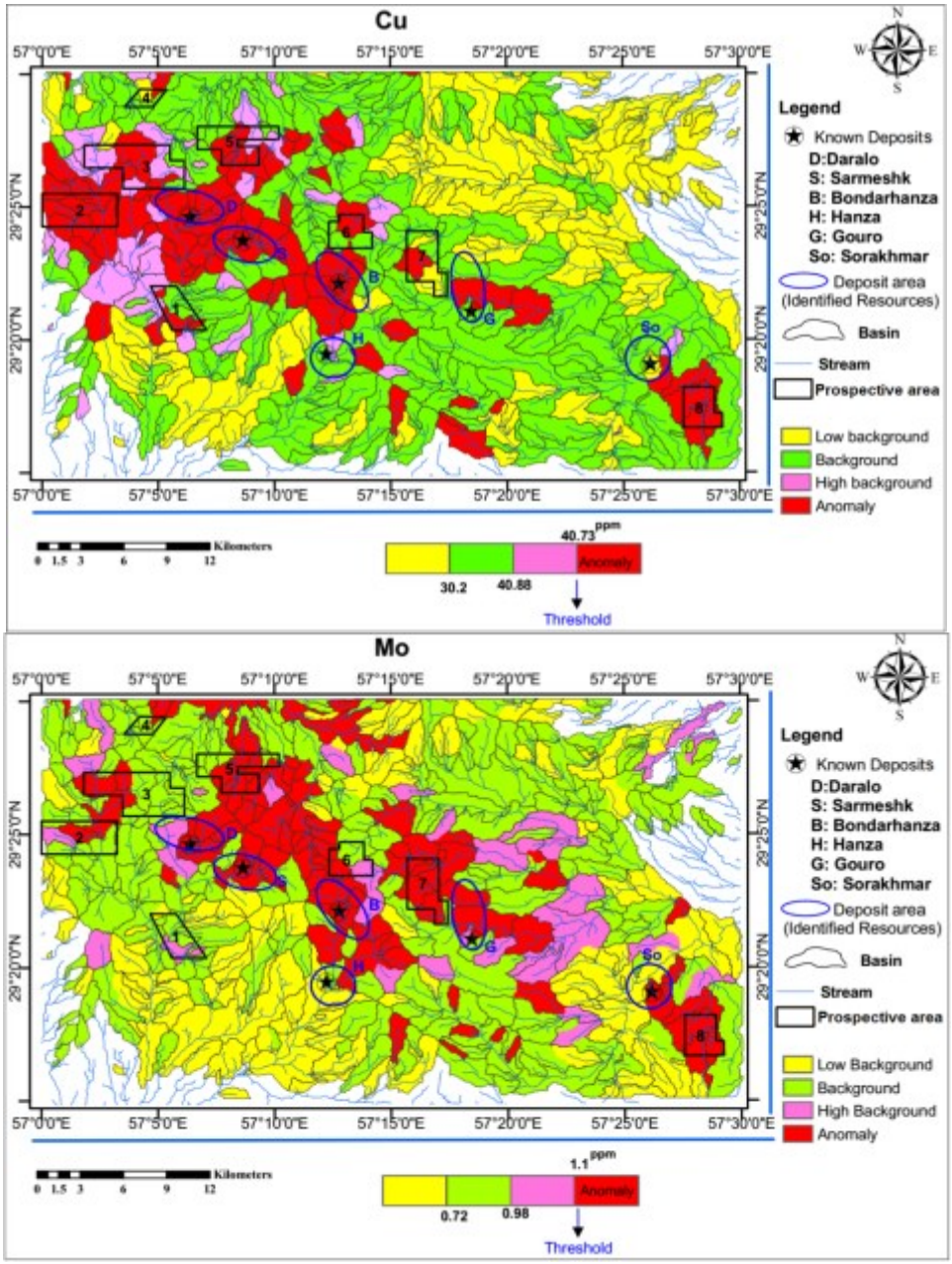

Figure 4. Copper and Molybdenum geochemical maps.

Table 2. The success percentage of MAD method to identify the sum of anomalous areas based on geochemical maps (Yes; identified, No: not identified).

	known porphyry copper deposit Area							new prospective Area									
	D*	S	B	G	H	So		1	2	3	4	5	6	7	8	Success rate	Efficiency
Cu	Yes	Yes	Yes	Yes	No	No		Yes	Yes	Yes	Yes	Yes	Yes	Yes	Yes	86 %	Very high
Mo	Yes	Yes	Yes	Yes	Yes	Yes		No	Yes	Yes	Yes	Yes	Yes	Yes	Yes	93 %	Very high

*Abbreviations of the known PCDs: D-Daralu, S-Sarmeshk, B-Bondar Hanza, G-Gouro, H-Hanza, S-Sorakhmar

4.2. Results of remote sensing data processing

Regional scale identification and mapping of hydrothermal alterations is an important preliminary step in mineral exploration [69, 79]. The satellite image processing was done to enhance the anomalous areas for both the proved PCDs and the newly-identified ones.

Data processing is performed to identify areas rich in kaolinite and sericite/muscovite. These are the key minerals for argillic and phyllic alteration zones, respectively. Distinguishing muscovite rich area can be a significant indicator for mapping the effect of hydrothermal alteration processes on related host rock [37, 80-82]. Experimental analysis shows that a 4-6-8 bands-colour composite is a good colour combination for distinguishing alteration zones [38]. ASTER False colour composite 468 (in RGB) images typically show argillic and phyllic alteration zones as red to pink tones and propylitic alteration zone as green tones (Figure 5) due to Al–OH (centered at ASTER band 6) and Fe–,Mg–O–OH (centered at ASTER band 8) absorption features, respectively [24, 31, 38]. Three BRs have been performed such as: (i) 4/5 band ratio for identifying kaolinite, (ii) 4/6 band ratio for identifying muscovite, and (iii) 4/7 band ratio for identifying jarosite [24, 38] in the supergene alteration zones. In the supergene zone, jarosite is the main secondary Fe^{3+} phase, and is formed under conditions of weathering (i.e. oxidation) in arid climates [83]. Jarosite is formed only in altered environments, while hematite is formed in both altered and unaltered (especially sedimentary rocks) environments. Therefore, in the identification of oxide-alterations associated with porphyry deposits, detection of jarosite is more important than hematite (e.g. b4/b7 in ASTER bands). The vegetation effect, due to the selection of band four as numerator, was first removed by subtracting 3/2 band ratio from all band ratios. Three BR ratios were assigned to RGB (red, green, and blue) colour combination. Then thresholds were selected using X+2s. In the resulted RGB, (R = [(4/5)-(3/2)], G = [(4/6)-(3/2)], and B = [(4/7)-(3/2)]), the area in white colour shows a response of band 5, band 6 (Al–OH), and band 7 (Fe–OH) (Figure 6), white areas are the alteration zones that are associated with porphyry system [38].

In addition to these three BRs (i) 7/6 band ratio for identifying muscovite, [37], (ii) band ratio of 5/6 for identifying kaolinite, and (iii) band ratio of 9/8 for identifying propylitic alteration zones [31, 37] have also been performed. Three BRs were assigned for RGB (red, green, and blue) colour combination to delineate argillic, phyllic and propylitic hydrothermal zones (Figure 7). Argillic alteration zone depicts as green and phyllic alteration zone as yellow to reddish yellow colours and propylitic alteration zone as light blue in the studied area. Three RBD ratios have adopted in this study; RBD5, RBD6, and RBD8. The RBD ratios have been derived based on [73] as RBD_5 = [(ASTER band 4 + ASTER band 6)/ ASTER band 5], RBD_6 = [(ASTER band 5 + ASTER band 7)/ ASTER band 6] and RBD_8 = [(ASTER band 7 + ASTER band 9)/ASTER band 8]. The vegetation effect has been eliminated from RBD5. Then thresholds were selected using X+2s. Three RBD ratios were assigned for RGB (R = RBD6, G = [(RBD5)-(3/2)], and B = RBD8) colour combination (Figure 8). Argillic alteration zone appears as bluish green and phyllic alteration zone as yellow colour, and propylitic alteration zone as blue and violet in RGB image.

RGB in Figure 6 is useful in showing argillic and phyllic hydrothermal alteration types. The white zones reflect the simultaneous presence of red, green, and blue bands with three key minerals of kaolinite, muscovite, and jarosite, respectively. The displayed white zones in the known deposit areas (especially Daralo, Sarmeshk, Gouro, and Sorakhmar) are consistent with the actual facts on the ground. The three key minerals in and around these deposits are widespread. FCC images show propylitic zone along with argillic and phyllic alteration zones in Figures 7 and 8. Amongst FCC images, the RGB in Figure 7 is the most useful in showing propylitic hydrothermal alteration.

According to the geological map, the blue areas are carbonate units, and the light blue (sky blue) areas are andesite-basalt with propylitic alteration in FCC image of band ratios 7/6 (R)-5/6 (G)-9/8 (B). A good discrimination has been created

between these two geological units by this image. In Figure 7, propylitic alteration with light blue colour (only the effect of 9/8 in the blue band) is well-revealed in these rocks but in Figure 8, these areas are mainly represented in violet colour (composition of red and blue bands) that is not consistent with the ground reality. In the propylitic environment, the presence of muscovite and montmorillonite minerals is very low. Therefore, the best FCC image to reveal the hydrothermal alteration zones that are associated with the porphyry deposits is [(4/5)-(3/2) in R] - [(4/6)-(3/2) in G] - [(4/7)-(3/2) in B]. The best image to show propylitic alteration zone along with argillic and phyllic zones is R-G-B of band rations 7/6-5/6-9/8.

For mineral prospectivity mapping of a deposit-type in an area, spatial datasets used are based on a conceptual model of prospectivity of that deposit-type. Then from individual spatial datasets (e.g. mineral alteration, distance to structures, geological complexity, geochemical signature, etc.) the corresponding evidential maps are generated, weighted, and integrated to delineate target areas [84]. Therefore, evaluating the relative importance of every evidential map derived from particular spatial datasets is a highly important exercise [85, 86]. In this regard, because the MAD method has a high ability to identify anomalous areas, the geochemical map obtained from this method can be considered as an evidential map. Furthermore, hydrothermal alteration zones are formed in a wide range of geological environments with hydrothermal mineral deposits, which can be the exploratory targets. In this research work, four hydrothermal alteration images were introduced, and each could be valid as an evidential map. However, the researcher should choose one as an evidential map. Evaluating and comparing four hydrothermal alteration images was performed based on the identification of the known significant anomalous areas (i.e. 14 anomalous areas). RGB in Figure 6 is useful in showing the argillic and phyllic hydrothermal alteration types in all the anomalous areas. However, the distinguished image to show propylitic alteration zone along with argillic and phyllic zones is R-G-B of band ratios 7/6-5/6-9/8 (Figure 7). It is noteworthy that RGB in Figure 5 is good in showing hydrothermal alteration types in all the anomalous areas. Therefore, choosing the best image depends on the expert's judgment and cannot extrapolate the results obtained from a processed image in an area to another. However, according to the authors' opinion, the best image (as the evidential map) is R-G-B of band ratios [(4/5)-(3/2)]-[(4/6)-(3/2)]-[(4/7)-(3/2)] (Figure 6).

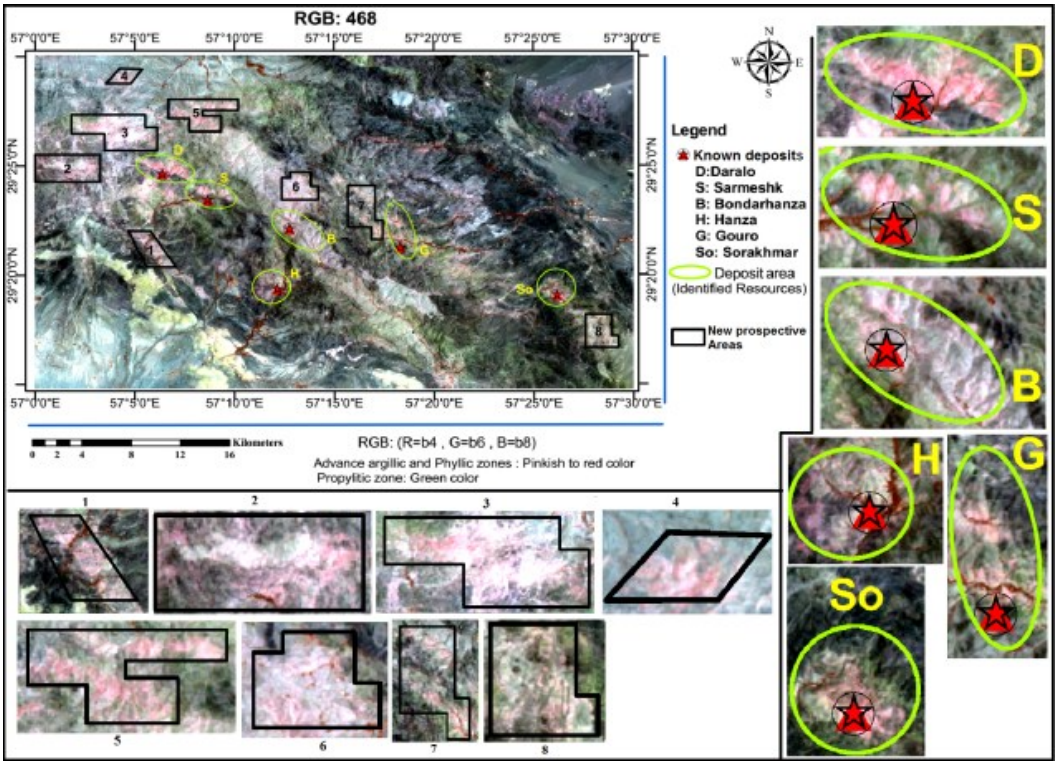

Figure 5. Demonstration of ASTER data processing in order to identify areas rich in kaolinite and muscovite, False-colour composite in RGB mode (R = 4, G = 6, B = 8). In this colour composite, propylitic alteration appears as green, and phyllic alteration zones with large quantities of Al-OH minerals are pinkish to yellowish in colour.

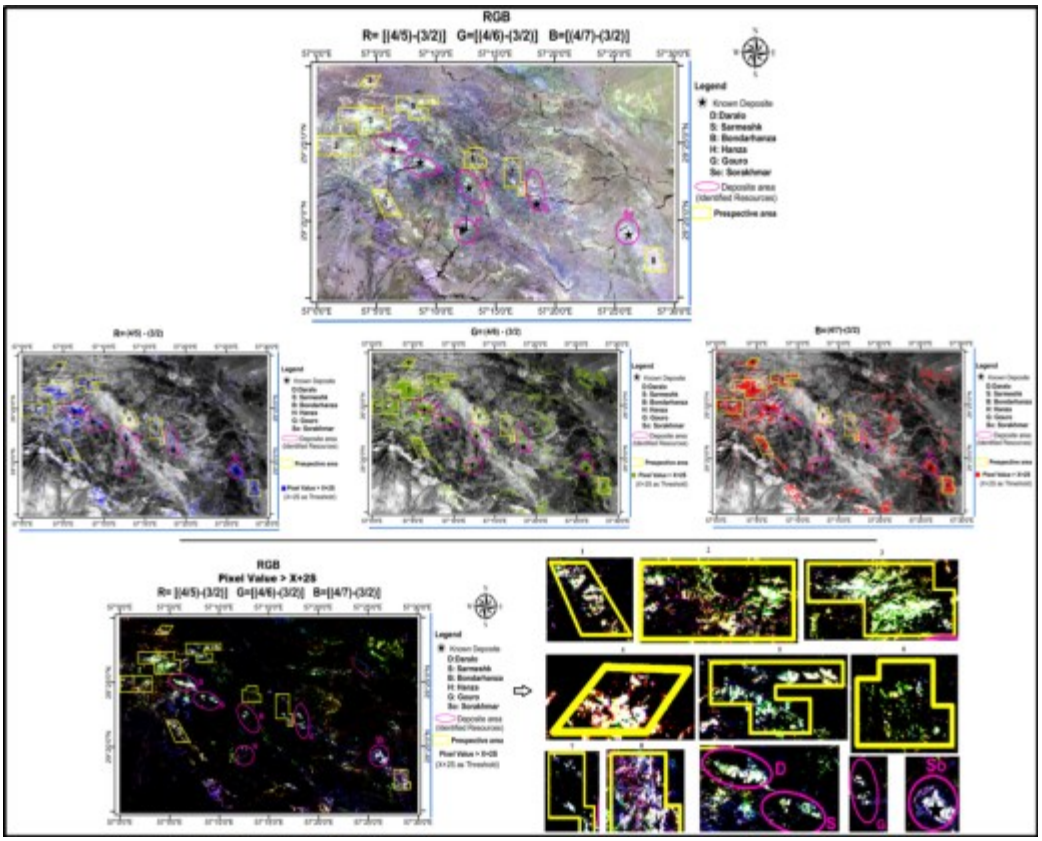

Figure 6. Demonstration of ASTER data processing in order to identify areas rich in kaolinite, muscovite, and jarosite, white area shows 2.16 $^{\mu m}$, 2.2 $^{\mu m}$, and 2.26 $^{\mu m}$ absorptions.

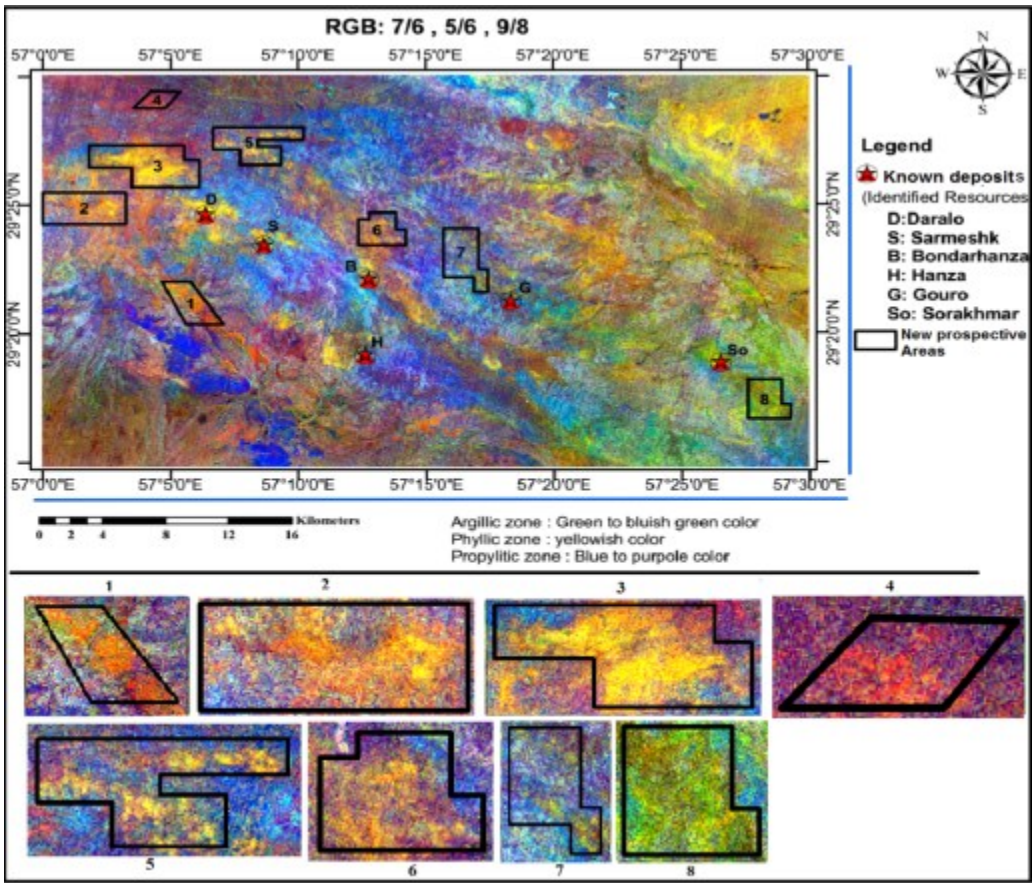

Figure 7. False-colour composite of band ratios (R=7/6, G=5/6, B= 9/8). Argillic alteration zones as green and phyllic alteration zones as yellow to reddish yellow colours and propylitic alteration zones as light blue.

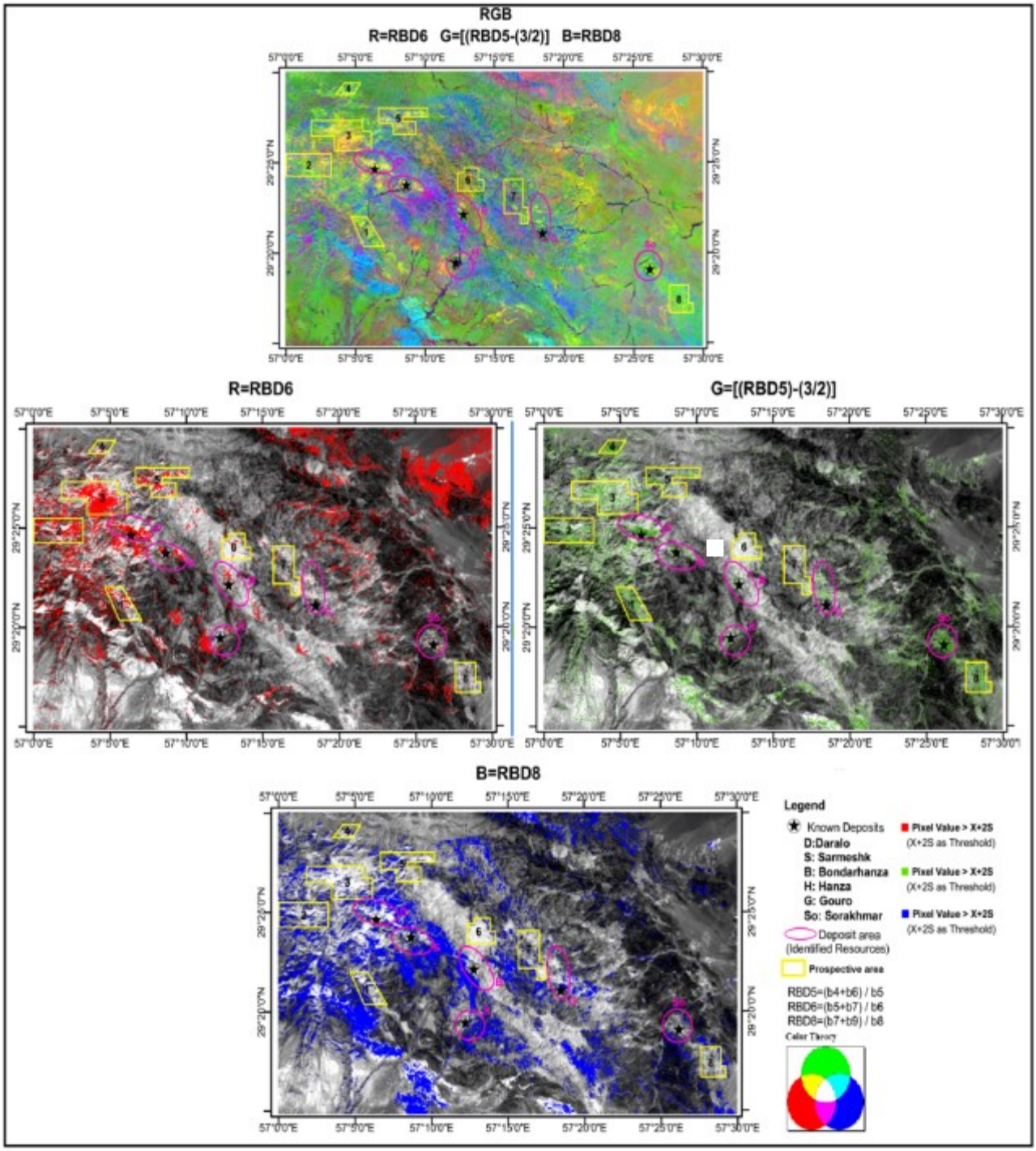

Figure 8. False-colour composite of RBD. Argillic alteration zone as bluish green and phyllic alteration zone as yellow colour.

5. Conclusions

1- The success rate can be used as assessment criteria to examine the effective processing techniques (i.e. the threshold estimation methods in the analysis of stream sediment geochemical datasets). In this research work, the success rate of the MAD method in identifying anomalous areas is very high for both Cu and Mo. Generally, the efficiency of this method in identifying anomalies, especially weak anomalies, is appropriate.

2- Given that the calculation of the MAD method is fast and convenient, hence, it is recommended in lieu of X+2S because it does not require a dataset to follow a normal distribution.

3- The geochemical map obtained from the MAD method as an evidential layer can be used to generate a mineral prospectivity map in combination with other exploratory data such as remote sensing and geophysics.

4- Image processing of ASTER satellite images, especially band ratios of ASTER images in R-G-B: [(b4/b5)-(b3/b2)] - [(b4/b6)-(b3/b2)] - [(b4/b7)-(b3/b2)], which were employed in this work had a high efficiency in mapping of argillic and phyillic alteration zones and it could be used as a valid criterion for regional exploration. In the Hanza region, six known deposits have been detected with obvious and widespread argillic and phyillic hydrothermal alterations.
5- False-colour composite of band ratios (R = b7/b6, G = b5/b6, B = b9/b8 of ASTER bands) is also an efficient image for detection of different type of hydrothermal alterations associated with porphyry deposits in the vegetated areas.
6- RBDs and band ratios have shown that hydrothermal alteration zones can be effectively enhanced in this semi-arid area.

References

[1]. Grunsky, E.C. (2006). The evaluation of geochemical survey data: data analysis and statistical methods using geographic information systems. In: J.R. Harris (Ed.), GIS for the Earth Sciences. Geological Association of Canada Special Publication. 44: 229-283.

[2]. Chudasama, B., Porwal, A., Álvarez, I.G., Sanchari Thakur, T. and Kreuzer, O.P. (2018). Calcrete-hosted surficial uranium systems in Western Australia: Prospectivity modeling and quantitative estimates of resources. Part 2- Prospectivity modeling and exploration targets. Ore Geol. Rev. (In press)

[3]. Parsa, M., Maghsoudi, A. and Yousefi, M. (2018). Spatial analyses of exploration evidence data to model skarn-type copper prospectivity in the Varzaghan region, NW Iran. Ore Geol. Rev. 92: 97-112.

[4]. Li, N., Xiao, K., Sun, L., Li, S.H., Zi, J., Wang, K., Song, Xi., Ding, J. and Li, C. (2018a) Part I: A resource estimation based on mineral system modelling prospectivity approaches and analogical analysis: a case study of the MVT Pb-Zn deposits in Huayuan region, China. Ore Geol. Rev. (In press)

[5]. Li, N., Xiao, K., Zhang, T., Song, X., Chen, Zh., Yin, J., Lou, D., Ding, J., Sun, L., Fan, J. and Li, C. (2018). A GIS-based tool for the China National Mineral Resource Assessment Initiative: A case study of gold deposits in the Bayan Obo Group, Inner Mongolia, China. Ore Geol. Rev. (In press)

[6]. Luo, D. and Zeng, G. (2018). Application and effects of singularity analysis in evaluating the denudation degree of Carlin-type gold deposits in southwest Guizhou, China. Ore Geol. Rev. 96: 164-180.

[7]. Sun, X., Zheng, Y., Wang, Ch., Zhao, Z. and Geng, X. (2016). Identifying geochemical anomalies associated with Sb–Au–Pb–Zn–Ag mineralization in north Himalaya, southern Tibet. Ore Geol. Rev. 73: 1-12.

[8]. Garousi Nezhad, S., Mokhtari, A.R. and Roshani Rodsari, P. (2017). The true sample catchment basin approach in the analysis of stream sediment geochemical data. Ore Geol. Rev. 83: 127-134.

[9]. Yang, L., Wang, O., Liu, H., Carranza, E.J.M., Li, G. and Zhou, D. (2017). Identification and mapping of geochemical patterns and their significance for regional metallogeny in the southern Sanjiang, China. Ore Geol. Rev. 90: 1042-4053.

[10]. Wang, W., Zhao, J., Cheng, Q. and Zhang, S.H. (2017). Spatially quantitative characterization of geological processes associated with polymetallic Sn-W mineralization in the Malipo mineral region, Southeastern Yunnan, China. Ore Geol. Rev. 91: 1147-1161.

[11]. Steenfelt, A., Kolb, J. and Thrane, K. (2016). Metallogeny of South Greenland: A review of geological evolution, mineral occurrences and geochemical exploration data. Ore Geol. Rev. 77: 194-245.

[12]. Zhou, S., Zhou, K., Cui, Y., Wang, J. and Ding, J. (2015). Exploratory Data Analysis and Singularity Mapping in Geochemical Anomaly Identification in Karamay, Xinjiang, China. J. Geochem. Explor. 154: 171-179.

[13]. Parsa, M., Maghsoudi, A., Yousefi, M. and Carranza, E.J.M. (2016). Multifractal interpolation and spectrumearea fractal modeling of stream sediment geochemical data: Implications for mapping exploration targets. J. Afr Earth Sci. 1-11.

[14]. Reimann, C., Filzmoser, P. and Garrett, R.G. (2005). Background and threshold: critical comparison of methods of determination. Sci Total Environ. 346: 1-16.

[15]. Carranza, E.J.M. (2009). Exploratory analysis of geochemical anomalies. In M. Hale (Ed.) Geochemical Anomaly and Mineral Prospectivity Mapping in GIS, Handbook of Exploration and Environmental Geochemistry 11, Elsevier, 351 P.

[16]. Asadi, H.H., Kianpouryan, S., JunLu, Y. and McCuaig, T.C. (2014). Exploratory data analysis and C–A fractal model applied in mapping multi-element soil anomalies for drilling: A case study from the Sari Gunay epithermal gold deposit, NWIran. J. Geochem. Explor. 145: 233-241.

[17]. Yang, Jie., Frederik, P.A. and Cheng, Q. (2015). Anovelfiltering technique for enhancing mineralization associated geochemical and geophysical anomalies. Comput. Geosci. 79: 94-104.

[18]. Wellmer, F.W. (1998). Statistical evaluations in exploration for mineral deposits, Springer New York. 379 P.

[19]. Hawkes, H.E. and Webb, J.S. (1962). Geochemistry in mineral exploration. New York and Evanston: Harper and Row. 415 P.

[20]. Tukey, J.W. (1977). Exploratory data analysis. Addison-Wesley, Reading.

[21]. Cheng, Q., Agterberg F.P. and Ballantyne, S.B. (1994). The separartion of geochemical anomalies from background by fractal methods. J. Geochem. Explor. 5: 109-130.

[22]. Ranjbar1, H., Shahriari1, H. and Honarmand, M. (2003). Comparison of ASTER and ETM+ data for exploration of porphyry copper mineralization: A case study of Sar Cheshmeh areas, Kerman, Iran. Map Asia Conference, © GISdevelopment.

[23]. Bedini, E. (2011). Mineral mapping in the Kap Simpson complex, central East Greenland, using HyMap and ASTER remote sensing data. Adv Space Res. 47: 60-73.

[24]. Di Tommaso, I.D. and Rubinstein, N. (2007). Hydrothermal alteration mapping using ASTER data in the Infiernillo porphyry deposit, Argentina. Ore Geol. Rev. 32: 275-290.

[25]. Gabr, S., Ghulam, A. and Kusky, T. (2010). Detecting areas of high-potential gold mineralization using ASTER data. Ore Geol. Rev. 38: 59-69.

[26]. Honarmand, M., Ranjbar, H. and Shahabpour, J. (2011). Application of Spectral Analysis in Mapping Hydrothermal Alteration of the Northwestern Part of the Kerman Cenozoic Magmatic Arc, Iran. J. Sci. I. R. Iran. 22: 221-238.

[27]. Pour, A.B. and Hashim, M. (2011). Identification of hydrothermal alteration minerals for exploring of porphyry copper deposit using ASTER data, SE Iran. Journal of Asian Earth Sciences. 42: 1309-1323.

[28]. Zhang, X., Micha, P. and Norman, D. (2007). Lithologic and mineral information extraction for gold exploration using ASTER data in the south chocolate mountains (California). Journal of Photography. 62: 271-282.

[29]. Beiranvand Pour, A. and Hashim, M. (2011). Identification of hydrothermal alteration minerals for exploring of porphyry copper deposit using ASTER data, SE Iran. Journal of Asian Earth Sciences. 42: 1309-1323.

[30]. Massironi, M.L., Bertoldi, P., Calafa, D., Visona, A., Bistacchi, C., Giardino, A. and Schiavo, B. (2008). Interpretation and processing of ASTER data for geological mapping and granitoids detection in the Saghro massif (eastern Anti-Atlas, Morocco). Geosphere. 4: 736-759.

[31]. Mars, J.C. and Rowan, L.C. (2010). Spectral assessment of new ASTER SWIR surface reflectance data products for spectroscopic mapping of rocks and minerals. Remote Sens Environ. 114: 2011-2025.

[32]. Van der Meer, F.D., van der Werff, H.M.A., van Ruitenbeek, F.J.A. and Hecker, C.A. (2012). Multi- and hyperspectral geologic remote sensing: A review. Int J Appl Earth Obs Geoinf. 14: 112-128.

[33]. Mohebi, A., Mirnejad, H., Lentz, D., Behzadi, M., Kani, A., Taghizadeh, H. and Dolati, A. (2015). Controls on porphyry Cu mineralization around Hanza Mountain, south-east of Iran: An analysis of structural evolution from remote sensing, geophysical, geochemical and geological data. Ore Geol. Rev. 69: 187-198.

[34]. Mars, J.C. and Rowan, L.C. (2006). Regional mapping of phyllic- and argillic-altered rocks in the Zagros magmatic arc, Iran, using Advanced Spaceborne Thermal Emission and Reflection Radiometer (ASTER) data and logical operator algorithms. Geosphere. 2: 161-186.

[35]. Tangestani, M.H., Mazhari, N., Ager, B. and Moore, F. (2008). Evaluating advance spaceborne thermal emission and reflection radiometer (ASTER) data for alteration zone enhancement in a semi-arid area, northern Shahr-e-Babak, SE Iran. International Journal of Remote Sensing. 29 (10): 2833-2850.

[36]. Khaleghi, M. and Ranjbar, H. (2011). Alteration Mapping for Exploration of Porphyry Copper Mineralization in the Sarduiyeh Area, Kerman Province, Iran, Using ASTER SWIR Data. Australian Journal of Basic and Applied Sciences. 5 (8): 61-69.

[37]. Beiranvand Pour, A. and Hashim, M. (2012). Identifying areas of high economic-potential copper mineralization using ASTER data in the Urumieh–Dokhtar Volcanic Belt, Iran. Advances in Space Research. 49: 753-769.

[38]. Alimohammadi, M., Alirezaei, S. and Kontak, D.J. (2015). Application of ASTER data for exploration of porphyry copper deposits: A case study of Daraloo–Sarmeshk area, southern part of the Kerman copper belt, Iran. Ore Geology Reviews. 70: 290-304.

[39]. Agard, P., Monié, P., Gerber, W., Omrani, J., Molinaro, M., Labrousse, L., Vrielynck, B.,Meyer, B., Jolivet, L. and Yamato, P. (2006). Transient, syn-obduction exhumation of Zagros blueschists inferred from P-T-deformation-time and kinematic constraints implications for Neotethyan wedge dynamics. Geophysical Research Letters. 111: B11401.

[40]. Bazin, D. and Hubner, H. (1968). Copper Deposits in Iran. Geol Survey of Iran. Behn, G., Camus, F., Carrasco, P., Ware, H., Aeromagnetic signature of porphyry coppersystems in northern Chile and its geologic implications. Economic Geology. 96: 239-248.

[41]. Berberian, F., Muir, I.D., Pankhurst, R.J. and Berberian, M. (1982). Late Cretaceous and early Miocene Andean-type plutonic activity in northern

Makran and Central Iran. Geological Society of London. 139: 605-614.

[42]. Djokovic, I., Dimitrijevic, M.N., Cvetic, S. and Dimitrijevic, M.D. (1973). Geological map of Iran sheet 7448-Sarduiye, scale 1:100,000.

[43]. Berberian, M. and King, G.C. (1981). Towards a paleogeography and tectonic evolution of Iran. Can J Earth Sci. 18: 210-265.

[44]. Shahabpour, J. (2005). Tectonic evolution of the orogenic belt in the region located between Kerman and Neyriz. Journal of Asian Earth Sciences. l24: 405-417.

[45]. Cooke, D.R., Hollings, P. and Walshe, J.L. (2005). Giant porphyry deposits: characteristics, distribution, and tectonic controls. Economic Geology. 100: 801-818.

[46]. Omrani, J., Agard, P., Whitechurch, H., Benoit, M., Prouteau, G. and Jolivet, L. (2008). Arc-magmatism and subduction history beneath the Zagros Mountains, Iran:A new report of adakites and geodynamic consequences. Lithos, 106: 380-98.

[47]. Sillitoe, R.H. (2010). Porphyry Copper Systems. Economic Geologists. 105: 3-41.

[48]. Aftabi, A. and Atapour, H. (1997). Geochemical and petrological characteristics of shoshonitic and potassic calcalkaline magmatism at Sarcheshmeh and Dehsiahan porphyry copper deposits, Kerman, Iran. Research Bulletin of Isfahan University. 9: 127-156 (in Persian).

[49]. Hassanzadeh, J. (1993). Metallogenic and tectonomagmatic events in the SE sector of the Cenozoic active continental margin of central Iran (Shahr e Babak area, Keman Province) Ph.D. Thesis University of California, Los Angeles, Los Angeles. 204 P.

[50]. Bonham-Carter, G.F. and Goodfellow, W.D. (1984). Autocorrelation structure of stream sediment geochemical data: interpretation of Zn and Pb anomalies, Nahanni River area, Yukon-Northwest Territories, Canada. In: Verly, G., David, M., Journel, A., Marechal, A. (eds.): Geostatistics for Natural Resources Characterization. Reidel Dordrecht. 2: 817-829.

[51]. Abdolmaleki, M., Mokhtari, A.R., Akbar, S., Alipour-Asll, M. and Carranza, E.J.M. (2014). Catchment basin analysis of stream sediment geochemical data: Incorporation of slope effect. J. Geochem. Explor. 140: 96-103.

[52]. Carranza, E.J.M. (2010). Catchment basin modeling of stream sediment anomalies revisited: incorporation of EDA and fractal analysis. Geochem. Explor. Environ. Anal. 10: 365-381.

[53]. Carranza, E.J.M. (2009). Geochemical anomaly and mineral prospectively mapping in GIS. In: Handbook of Exploration and Environmental Geochemistry, vol. 11. Elsevier, Amsterdam.

[54]. Carranza, E.J.M. and Hale, M. (1997). A catchment basin approach to the analysis of reconnaissance geochemical-geological data from Ably Province, Philippines. J. Geochem. Explor. 60: 157-171.

[55]. Templ, M., Filzmoser, P. and Reimann, C. (2008). Cluster analysis applied to regional geochemical data: Problems and possibilities. Appl Geochem. 23: 2198-2213.

[56]. Zuo, R. (2014). Identification of weak geochemical anomalies using robust neighborhood statistics coupled with GIS in covered areas. J. Geochem. Explor. 136: 93-101.

[57]. Reimann, C. and Garrett, R.G. (2005). Geochemical background-concept and reality. Science of the Total Environment. 350: 12-27.

[58]. Lowell, J.D. and Guilbert, J.M. (1970). Lateral and vertical alteration-mineralization zoning in porphyry ore deposits. Economic Geology. 65 (4): 373-408.

[59]. Abrams, M.J., Brown, D., Lepley, L. and Sadowski, R. (1983). Remote sensing for porphyry copper deposits in southern Arizona. Economic Geology. 78 (4): 591-604.

[60]. Spatz, D.M. and Wilson, R.T. (1995). Remote sensing characteristics of porphyry copper systems, western America Cordillera, in Pierce, F.W., and Bolm, J.G., eds.: Arizona Geological Society Digest. 20: 94-108

[61]. Sadeghi, B., Khalajmasoumi, M., Afzal, P., Moarefvand, P., Yasrebi, A.B., Wetherelt, A., Foster, P. and Ziazarifi, A. (2013). Using ETM+ and ASTER sensors to identify iron occurrences in the Esfordi 1:100,000 mapping sheet of Central Iran. J. Afr. Earth Sci. 85: 103-114.

[62]. Pirajno, F. (2009). Hydrothermal Processes and Mineral Systems (Chapter 2: Hydrothermal Processes and Wall Rock Alteration), Springer Science+Business Media B.V, 1250 P.

[63]. Ben-Dor, E., Kruse, F.A., lefkoff, A.B. and Banin, A. (1995). Comparison of three calibration techniques for utilization of GER 63-channel aircraft scanner data of Makhtesh Ramon, Nega, Israel. Int. J. Rock Mech. Min. Sci. 32: 164A.

[64]. Legg, C.A. (1994). Remote sensing and geographical information system geological mapping, Mineral Exploration and Mining. New York, Ellis Horwood. 166 P.

[65]. Vincent, R.K. (1997). Fundamentals of geological and environmental remote sensing. Prentice Hall, 370 P.

[66]. Khosroshahizadeh, S., Pourkermani, M., Almasian, M., Arian, M. and Khakzad, A. (2016). Lineament Patterns and Mineralization Related to Alteration Zone by Using ASAR-ASTER Imagery in Hize Jan-Sharaf Abad Au-Ag Epithermal Mineralized Zone (East Azarbaijan—NW Iran). Open Journal of Geology. 6: 232-250.

[67]. Aboelkhair, H., Ninomiya, Y., Watanabe, Y. and Sato, I. (2010). Processing and interpretation of ASTER TIR data for mapping of rare-metal-enriched albite granitoids in the Central Eastern Desert of Egypt. J. Afr. Earth Sci. 58: 141-151.

[68]. Abdelnasser, A., Kumral, M., Zoheir, B., Karaman, M. and Weihed, P. (2018). REE geochemical characteristics and satellite-based mapping of hydrothermal alteration in Atud gold deposit, Egypt. J. Afr. Earth Sci. 145: 317-330.

[69]. Mahanta, P. and Maiti, S. (2018). Regional scale demarcation of alteration zone using ASTER imageries in South Purulia Shear Zone, East India: Implication for mineral exploration in vegetated regions. Ore Geol. Rev. doi: https://doi.org/10.1016/j.oregeorev.2018.07.028 (In Press)

[70]. Ibrahim, W.S., Watanabe, K. and Yonezu, K. (2016). Structural and litho-tectonic controls on Neoproterozoic base metal sulfide and gold mineralization in North Hamisana shear zone, South Eastern Desert, Egypt: The integrated field, structural, Landsat 7 ETM+and ASTER data approach. Ore Geol. Rev. 79: 62-77.

[71]. Inzana, J., Kusky, T., Higgs, G. and Tucker, R. (2003). Supervised classifications of Landsat TM band ratio images and Landsat TM band ratio image with radar for geological interpretations of central Madagascar. J. Afr. Earth Sci. 37: 59-72.

[72]. Rowan, L.C. and Mars, J.C. (2003). Lithologic mapping in the Mountain Pass, California area using Advanced Spaceborne Thermal Emission and Reflection Radiometer (ASTER) data. Remote Sens Environ. 84: 350-366.

[73]. Khan, S.D. and Mahmood, K. (2008). The application of remote sensing techniques to the study of ophiolites. Earth Sci Rev. 89: 135-143.

[74]. Amer, R., Kusky, T. and Ghulam, A. (2010). Lithological mapping in the Central Eastern Desert of Egypt using ASTER data. J. Afr. Earth Sci. 56: 75-82.

[75]. Crowley, J.K., Brickey, D.W. and Rowan, L.C. (1989). Airborne imaging spectrometer data of the Ruby Mountains, Montana: mineral discrimination using relative absorption band-depth images. Remote Sens Environ. 29: 121-134.

[76]. Ziaii, M., Carranza, E.J.M. and Ziaei, M. (2011). Application of geochemical zonality coefficients in mineral prospectivity mapping. Comput. Geosci. 37: 1935-1945.

[77]. Ziaii, M., Pouyan, A.A. and Ziaei, M. (2009). Neuro-fuzzy modelling in mining geochemistry: identification of geochemical anomalies. J. Geochem. Explor. 100: 25-36.

[78]. Ziaii, M., Doulati, F., Ziaei, M. and Soleymani, A. (2012). Neuro-fuzzy modeling based genetic algorithms for identification of geochemical anomalies in mining geochemistry. Appl Geochem. 27: 663-676.

[79]. Abrams, M. and Hook, S.J. (1995). Simulated ASTER data for geologic studies. IEEE Transactions on Geoscience and remote sensing. 33: 1-3.

[80]. Abrams, M. (2002). ASTER user handbook. Jet Propulsion Lab.

[81]. Van Ruitenbeek, F.J.A., Pravesh, D. and Van der Meer, F.D. (2006). Mapping white micas and their absorption wavelengths using hyperspectral band ratios. Remote Sens Environ. 102: 211-222.

[82]. Sillitoe, R.H. (1973). The tops and bottoms of porphyry copper deposits: Economic Geology. 68: 799-815.

[83]. Murray, J., Kirschbaum, A., Dold, B., Mendes Guimaraes, E. and Pannunzio Miner, E. (2014). Jarosite versus Soluble Iron-Sulfate Formation and Their Role in Acid Mine Drainage Formation at the Pan de Azúcar Mine Tailings (Zn-Pb-Ag), NW Argentina. Minerals. 4: 477-502.

[84]. Yousefi, M. and Carranza, E.J.M. (2015). Prediction-area (P-A) plot and C-A fractal analysis to classify and evaluate evidential maps for mineral prospectivity modeling. Computers & Geosciences. 79: 69-81.

[85]. Yousefi, M. and Carranza, E.J.M. (2015). Fuzzification of continuous-value spatial evidence for mineral prospectivity mapping. Computers & Geosciences. 74: 97-109.

[86]. Ghezelbash, R., Maghsoudi, A. and Carranza, E.J.M. (2019). Mapping of single-and multi-element geochemical indicators based on catchment basin analysis: Application of fractal method and unsupervised clustering models. J. Geochem. Explor. 199: 90-104.

تعیین آنومالی‌های ذخایر مس پورفیری منطقه هنزا از طریق تحلیل داده‌های ژئوشیمیایی و چند طیفی سنجش از دور

امیرحبیب نیا، غلامرضا رحیمی پور* و حجت الله رنجبر

بخش مهندسی معدن، دانشگاه شهید باهنر کرمان، ایران

ارسال ۲۰۱۹/۳/۱۶، پذیرش ۲۰۱۹/۵/۱۳

* نویسنده مسئول مکاتبات: rahimipour@uk.ac.ir

چکیده:

منطقه هنزا در بخش جنوبی کمربند فلزی ارومیه- دختر در جنوب ایران واقع شده است. این منطقه شامل شش کانسار شناخته شده مس پورفیری است و از دیدگاه ژئوشیمیایی به عنوان یک منطقه معدنی محسوب می‌شود. هدف از این پژوهش، بررسی تکنیک‌های پردازش مؤثر در تجزیه و تحلیل داده‌های ژئوشیمیایی رسوبات رسوبی و تصاویر ماهواره‌ای ASTER است. روش‌های پردازش منجر به شناسایی هشت محدوده امیدبخش جدید شده است. روش ژئوشیمیایی با هدف ارائه نقشه‌های ژئوشیمیایی تک متغیره است. نقشه‌برداری ژئوشیمیایی رسوبات آبراهه‌ای برای Cu و Mo با استفاده از رویکرد حوضه آبریز بالادست هر نمونه انجام می‌شود. نقشه‌های ژئوشیمیایی حاصل از این رویکرد در چهار کلاس طبقه‌بندی شدند. طبقه‌بندی کلاس‌ها مرتبط با چارک اول، چارک سوم و مقادیر آستانه به دست آمده از روش MAD انجام شده است. تکنیک‌های ترکیب رنگی کاذب و نسبت باندی به عنوان دو روش شناخته شده برای پردازش تصاویر باندی ASTER در منطقه مورد مطالعه بکار گرفته شدند. هشت محدوده امید بخش جدید با کانی سازی ممکن از تجزیه و تحلیل داده‌های ژئوشیمیایی حاصل شده است. همچنین تکنیک‌های پردازش تصویر در داده‌های چند طیفی ASTER نشان می‌دهند که دگرسانی هیدروترمال وسیع مرتبط با ذخایر پورفیری هم در محدوده شش کانسار شناخته شده و هم هشت محدوده امید بخش جدید وجود دارد.

کلمات کلیدی: ناحیه هنزا، کمربند متالوژنیک ارومیه- دختر، روش انحراف مطلق میانه، نقشه‌برداری ژئوشیمیایی، کانسارهای مس پورفیری، ترکیب رنگی کاذب.